

We are IntechOpen, the world's leading publisher of Open Access books Built by scientists, for scientists

6,900

Open access books available

186,000

International authors and editors

200M

Downloads

Our authors are among the

154

Countries delivered to

TOP 1%

most cited scientists

12.2%

Contributors from top 500 universities



WEB OF SCIENCE™

Selection of our books indexed in the Book Citation Index
in Web of Science™ Core Collection (BKCI)

Interested in publishing with us?
Contact book.department@intechopen.com

Numbers displayed above are based on latest data collected.
For more information visit www.intechopen.com



Wetland Monitoring Using Unmanned Aerial Vehicles with Electrical Distributed Propulsion Systems

Esteban Valencia, Víctor Alulema and Darío Rodríguez

Abstract

The inspection of wetlands in the Ecuadorian highlands has gained importance due to the environmental issues linked to the growth of human activities and the expansion of the agricultural and livestock frontiers. In this sense, unmanned aerial vehicles (UAVs) have been amply used in monitoring activities such as the supervision of threatened ecosystems, where cyclic measurements and high-resolution imagery are needed. However, the harsh operating conditions in the Andean highlands and sensitive ecosystem restrictions demand efficient propulsion configurations with low environmental impact. Electrical distributed propulsion (EDP) systems have surged as a forefront alternative since they offer benefits in both the propulsive and aerodynamic performance of fixed-wing UAVs. In this chapter, an EDP system is sized for a design point at the Andean operating conditions. Thereafter, two propulsion configurations were established based on off-the-shelf components, and their performance was characterized through analytical approaches. These results highlight the trends in power consumption and performance when the number of propulsors is increased. A significant contribution of this work is to exhibit important patterns in the performance of electric propulsion by using commercial components, and to set the operating limitations that can be further explored for analogous configurations in larger UAVs.

Keywords: unmanned aerial vehicles, distributed propulsion, electrical propulsion, blended wing body, wetland monitoring

1. Introduction

The Andean region, which comprises paramos¹ [1] and wetlands, is considered a biodiversity hotspot that contains about one-sixth of earth's plant life [2, 3]. This extension of land is of great importance, since it represents the main water reservoir for major cities in Colombia, Ecuador, and Peru [4, 5]. Both wetlands and paramos

¹ A paramo is a Neotropical high mountain biome with a vegetation composed mainly of giant rosette plants, shrubs, and grasses.

are endangered ecosystems, and, hence, efficient and suitable monitoring solutions are urgently needed. In this way, different monitoring techniques including satellite imagery and the use of high-resolution cameras mounted on manned airplanes have been utilized. Nonetheless, the aforesaid methods are not commonly affordable because they are costly and require long setup times.

The advent of unmanned aerial vehicles (UAVs) has encouraged periodical and low-cost management of threatened ecosystems through real-time data acquisition. The incursion of aerial platforms into forestry remote sensing [6] has had a positive impact thanks to the usage of high-resolution sensors [7, 8] to gather data regarding flora health, species inventory, or mapping in a periodic way. In this respect, multicopters have been seen as the first option for monitoring; however, their low autonomy limits the area covered per flight. Conversely, fixed-wing UAVs have been introduced to overfly larger areas. The imagery provided by these tools has been collected using different payloads, ranging from basic RGB cameras to sophisticated radars. Nevertheless, the time employed for a specific mission profile is higher when operating at the Andean highlands because of the harsh atmospheric conditions, which constrain the UAV autonomy and performance.

Commercial UAVs usually perform under sea level conditions with low wind gusts (lower than 16 m/s) and higher air density. This denotes that an improvement in some UAV subsystems is required to tailor them for high-altitude monitoring applications [9, 10]. Among the different characteristics that need to be upgraded to enhance the UAV performance, the following can be summarized: robust flight control system able to withstand the strong wind gusts (18 m/s), aerodynamic and high volumetric fuselage to store the avionics and payload, and high-efficient and eco-friendly propulsion system, which reduces energy consumption. The two latter options are linked, and, thus, their implementation into the conceptual design requires the assessment of their suitability to explore synergies for a more efficient UAV configuration.

The purpose of the present chapter is to investigate the performance of an electric-powered blended wing body (BWB)² UAV deployed on the aforesaid ecosystems. This baseline configuration has been selected based on previous research [11], where it has been found that BWB configurations offer high volumetric efficiency while providing good aerodynamic performance [12] as a result of the elliptical lift distribution improvement over the whole airframe [13–15]. Furthermore, the BWB model facilitates the integration of different propulsion architectures, which results in a broader spectrum of configurations for distributed propulsion [16].

Regarding the power source, the electric option has been seen attractive because of the reduction of polluting gas emissions, moderate cost, lighter weight, and high reliability. In the next section, a deeper explanation about the propulsion configuration for this conceptual design is described.

2. UAV design methodology

2.1 Distributed electric propulsion

Reconnaissance and surveillance of endangered environments through over-flight missions require short setup time, versatility, and noise mitigation. In this sense, electric propulsion has emerged as a reliable and potential solution to

² A BWB is a tailless aircraft design that integrates the fuselage and the wings through blended cross sections in a single body.

accomplish the aforesaid requirements thanks to its high-efficiency, moderate cost, and eco-friendly essence. Nonetheless, the capacity of commercial batteries remains to be an issue because of their lower energy density compared with their counterpart, the fossil fuels [17, 18].

The distributed propulsion is a revolutionary technology that seeks to reduce the noise and weight of an aircraft by means of replacing large propulsors with a moderate amount of small ones along the airframe [16] as depicted in **Figure 1**. This offers the possibility of increasing the propulsive efficiency because a larger propulsive area is considered, which in turn, implies a lower jet velocity. Its application on small fixed-wing UAVs has not been formally studied³ [19], and, consequently, the present chapter aims to assess the performance of small UAV configurations with electric distributed propulsion. The study will focus mainly on power consumption and performance improvements to demonstrate the feasibility of employing this technology in small UAVs. Propulsive efficiency has not been considered as a figure of merit in the present study, because of the low operating speeds and the electrical propulsion system, where the use of this parameter does not capture well the improvement in the aircraft performance, as it does for turbofan engines.

It is important to note that distributed propulsion may offer other numerous benefits such as the elimination of the aircraft control surfaces (thrust vectoring), flexible maintenance, decrease in noise, and reduction in aircraft weight through inlet-wing integration [20]. The study of these advantages is beyond the scope of the present work, since this chapter is aimed at setting the basic conceptual configurations and assessing their suitability for the case study. Nonetheless, these various features will be implemented in further research, where the selected conceptual configurations will be assessed using a more holistic perspective.

For the assessment of suitable UAV configurations for wetland monitoring, parametric sizing and aerodynamic assessment approaches were implemented into the conceptual design stage. Then, a brief insight about the influence of electric distributed propulsion into the performance of the UAV configuration using a semiempirical approach is exposed. In the next sections, initial sizing and modelling of the UAV systems are further explained.

2.2 Initial sizing

The design procedure starts by defining the mission requirements such as flight altitude, velocities, and payload sensors. In this sense, a precise study of wetlands and paramos demands the usage of special sensors applied in monitoring activities such as crop scouting, precision agriculture, surveillance, and air quality

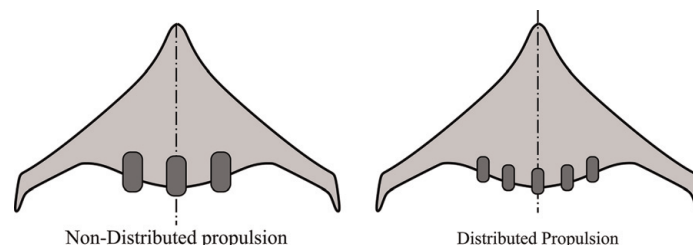


Figure 1.
Difference between distributed and non-distributed propulsion in a BWB.

³ Distributed propulsion configurations have been explored by hobbyists using mainly empirical assessments.

Main camera	Mass [g]	Resolution [MP]
Logitech C510	225	8
Canon PowerShot S60	230	5
Kodak Professional DCS Pro Back	770	16
Sony DSC-R1	929	10.3

Table 1.
Monitoring sensors applied for wetlands and forestry [21–25].

monitoring. Some sensors used in these monitoring tasks are listed in **Table 1**. In this work, the payload’s weight was assumed to be 1 kg for practical purposes

Next, the UAV layout is carried out, and main aircraft characteristics such as preliminary weight (W_{TOP}), wing planform area (S), and preliminary power required (P_{RP}) are delineated through the constraint analysis technique [26, 27]. This method consists of a matching plot that allows defining the design space of the aircraft depending on their performance requirements such as stall speed, maximum speed, takeoff run, and ceiling altitude [28]. The outcomes of this design stage represent the general characteristics of a preliminary aircraft architecture and will be employed to size other parts.

Afterwards, the wing shape is outlined by defining its geometrical parameters and sectional airfoils [26, 29]. The wing geometry was set according to technical and semiempirical correlations [18], and then, the obtained results were contrasted with corresponding data of commercial UAVs with similar characteristics [6]. In this way, the aerodynamic assessment was accomplished through the employment of the open-source Athena Vortex Lattice (AVL) software which incorporates the vortex lattice method (VLM) [30]. On the other hand, due to the lack of suitable analytical methods to calculate the weight of small UAV configurations, the preliminary weight was estimated as a function of the internal volume and the structural material’s density of the aircraft [26].

At the end of this stage, the external shape of a conceptual model is obtained. Thereafter, it is necessary to define a proper propulsion system through the match of the thrust required and the thrust available. Finally, the weight of the resulting architecture is assessed through a refined model that takes into account the propulsion system and the power source weight. **Figure 2** depicts the road map of the methodology employed to generate and characterize a conceptual BWB UAV model. It is worth to mention that all the symbols utilized along the chapter are reported in the nomenclature section at the end.

2.3 Propulsion modeling

The main function of aircraft propulsion systems is to generate enough thrust to overcome the drag and maintain a steady flight. For this work, firstly, suitable propellers were selected based on operating conditions and performance requirements of the UAV model. Then, the rest of propulsion elements (motor, electronic speed control and battery) was outlined based on propeller’s characteristics. Finally, the established propulsion set is evaluated to verify that both the power and the thrust available satisfy the requirements for cruise condition. It is important to mention that, at this conceptual stage, the distortion and momentum drag reduction of the incoming flow to the propeller has not been considered and will be studied in future work.

The propellers are commonly characterized by the thrust (C_T) and power (C_P) coefficients through semiempirical models at early stages of design [31]. For this

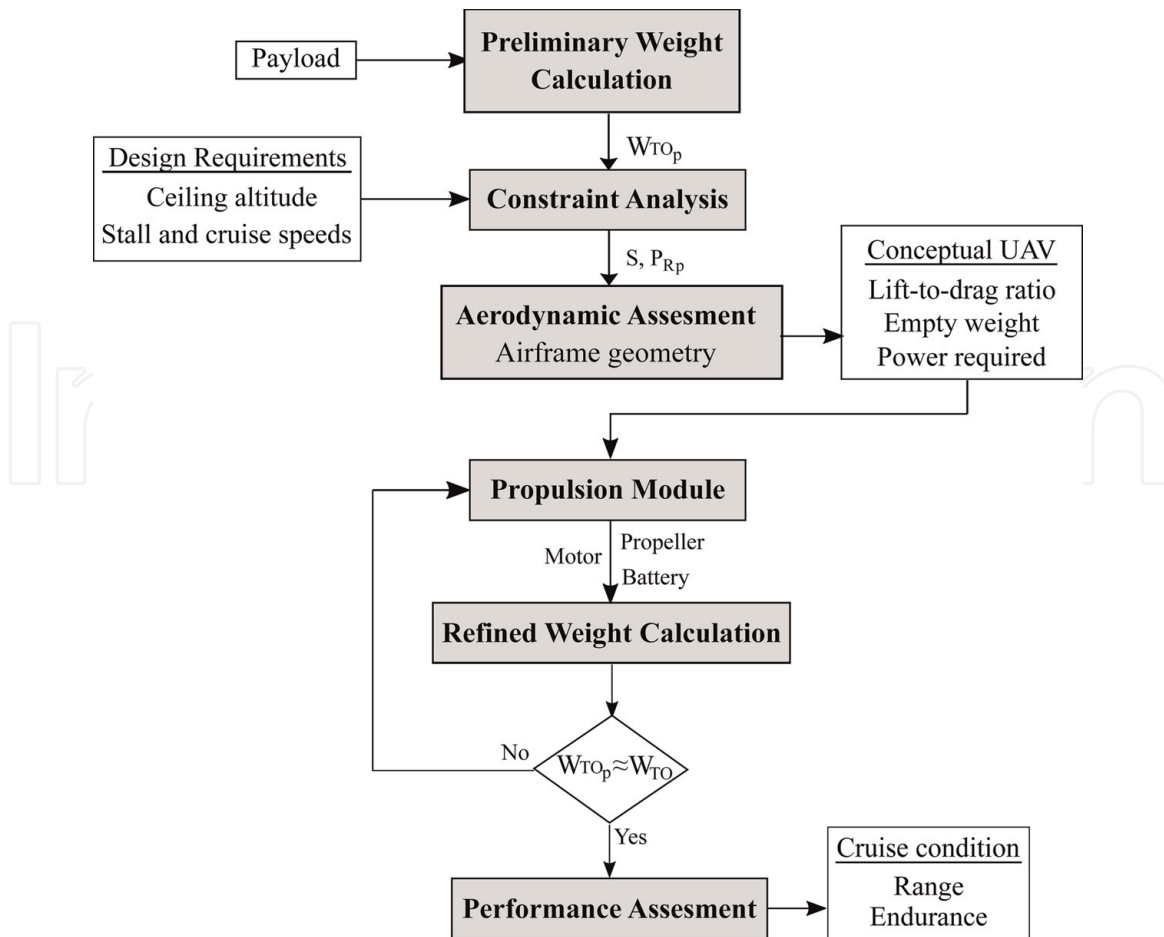


Figure 2.
 General methodology of initial aircraft sizing.

study, the aforesaid parameters were obtained from an experimental database of low Reynolds propellers [32] by using the advance ratio (J) as the key driver for the selection routine. This latter parameter relates the freestream velocity, the propeller diameter (ϕ_{prop}), and its rotational speed (ω). For this work, the freestream velocity was set according to the desired cruise speed. In this way, the proposed method involves an iterative scheme that consists of estimating the thrust and power generated by a preselected propeller through the variation of ϕ_{prop} and ω for the desired freestream velocity (V_c). The iterative loop stops when the thrust and power required are met by a certain configuration. Finally, these results were used to select appropriate electric motors and batteries which can adapt well to the design requirements. This semiempirical scheme was preferred since most of the available techniques [34, 35] are focused on large propeller assessment and, hence, they present limitations for their implementation into small aerial platforms.

Brushless electric motors are commonly employed for small UAVs considering their simple design, potential to downsize, little maintenance, and independent performance of the flight altitude. In addition, their purely inductive nature and their outrunner configuration (rotor with magnets that surrounds the fixed coils of the stator) enable them to generate high torque at a low rotational speed, eliminating the need of a gearbox and facilitating their integration and test at early stages of UAV design [18, 36]. In this context, appropriate motors were outlined based solely on basic parameters provided by manufacturers like rotational speed and torque. The selected motor must be able to generate the torque required by the propeller for its adequate functioning at a certain rotational speed [37]. Once a motor has been

selected, various operating parameters like no-load current, voltage constant, and internal resistance, together with torque and rotational speed that were taken from the datasheets, were employed to estimate the required voltage (U_m) and current (I_m) of the motor [36].

The motor current (I_m) is then employed to select a proper electronic speed control (ESC) device and a lithium-polymer (LiPo) battery. It is important to highlight that batteries for small UAVs are almost exclusively lithium-based because they offer high capacity, low weight, and high discharge rates [38]. For the battery selection, two different scenarios were explored in this work. The first consisted of defining a nominal battery capacity based on commercial off-the-shelf devices to estimate the flight endurance. The second scenario aims to determine a suitable battery by giving a target endurance. This latter approach was employed to assess the maximum endurance that could be achieved by the UAV, without the constraints of off-the-shelf electronic components. **Figure 3** illustrates the road map to establish the electric propulsion system during the conceptual design stage.

Once the propulsion system and the aircraft external shape have been framed, it is necessary to estimate the UAV total weight in a more refined and accurate way. This value is then contrasted with the admissible weight stated in the design requirements. Since typical procedures are focused on civil aviation, their application cannot be extended to small aerial platforms. Instead, this work proposes a method that individually accounts for the airframe, propulsion system, battery, and payload weights and then adds each contribution to obtain the total weight as stated in Eq. (1).

The structural weight of the airframe was calculated with respect to the fuselage internal volume and the material's density. The former was estimated through the convex hull method [39], and high-density foam was assumed as the major airframe material [26]. The weight of remaining components from Eq. (1) was readily obtained from manufacturer's datasheets.

$$W_{TO} = W_{airframe} + W_{propulsion} + W_{payload} + W_{battery} [N] \quad (1)$$

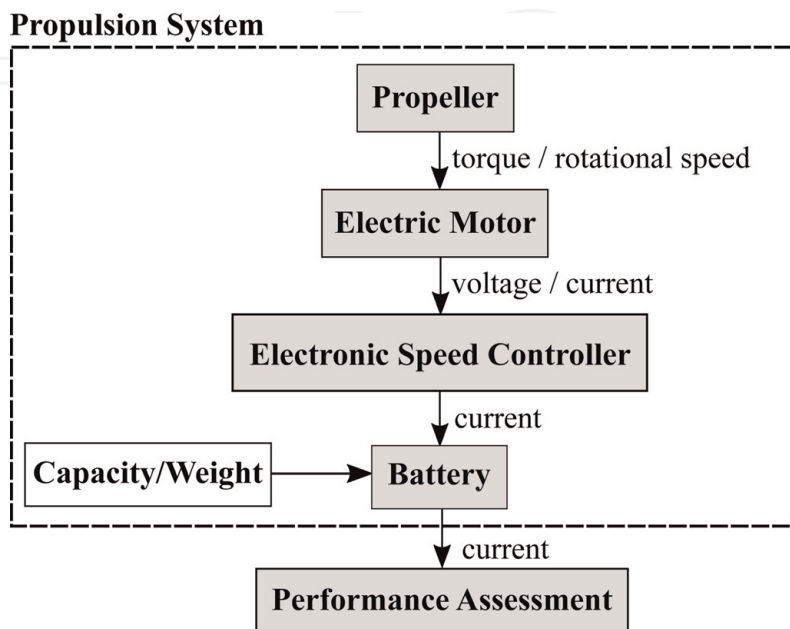


Figure 3. Electric propulsion definition and performance assessment methodology.

2.4 Performance evaluation

The performance analysis is an engineering discipline that relies on inputs from aerodynamic and propulsion assessments. In this sense, the performance evaluation aims to verify if a propulsion set (battery, motor and propeller) meets the mission requirements such as endurance and range. For this purpose, both the power required (P_R) and the power available (P_A) are determined. The former depends on the weight and the aerodynamic efficiency of an aircraft, while P_A depends on the propulsion system and its power source [35].

The power required (P_R) is calculated by means of Eq. (2) [34, 35], where ρ_{alt} is the air density at a desired altitude, S is the planform wing area, W_{TO} is the takeoff gross weight, and C_D and C_L are the drag and lift aerodynamic coefficients. Note that W_{TO} and S were previously defined in the initial sizing phase through the constraint analysis and the aerodynamic coefficients were estimated through the employment of the AVL software and parametric characterization [40]. This term represents the power required for steady cruise condition. However, the target power available (P_A) must be greater than P_R to consider a more demanding flight condition such as the takeoff phase. This excess of power is linked to the rate of climb (RC) as Eq. (3) shows [35]:

$$P_R = \sqrt{\frac{2}{\rho_{alt} \cdot S}} (W_{TO}^{3/2}) \left(\frac{C_D}{C_L^{3/2}} \right) [W] \quad (2)$$

$$P_A = P_R + RC \cdot W_{TO} [W] \quad (3)$$

The power available (P_A), which depends on the propeller, motor, and battery characteristics, was estimated through analytical relationships regarding non-dimensional coefficients (C_T , C_P , and J) [35]. The computed value of P_A was verified to be greater or equal to P_R in order to guarantee that the aircraft reaches the absolute ceiling altitude⁴ at the desired rate of climb as explained before. Note that P_R will be less for the cruise condition because the airplane is not climbing anymore and, thus, the excess of power is zero. Finally, for the distributed propulsion case, the total power available is estimated by multiplying the number of propellers by their generated power, respectively.

It is important to highlight that the battery must provide a greater power than P_A to account for energy losses as shown in Eq. (4), where η_{prop} represents the propeller efficiency, η_e is the efficiency of the electric set (motor, electronic speed driver and battery), and P_{bat} is the power supplied by the battery:

$$P_A = \eta_{prop} \eta_e P_{bat} [W] \quad (4)$$

The endurance and range are the key performance parameters because they reflect the time and distance that the aircraft is able to fly without recharging. Their estimation for electric-powered airplanes through analytical models has not received special attention because the devices for the efficient energy storage are still under development and research. Nevertheless, few authors have introduced distinct and elaborated methods to predict the aforesaid parameters from aerodynamic characteristics and battery working conditions [38, 41].

For this case, a simplified but good enough approach has been employed to estimate the endurance and range [36]. This method assumes that the voltage

⁴ This term is referred to the absolute maximum altitude that the aircraft can ever maintain level flight, i.e., the RC is zero [26].

remains constant and the battery capacity is decreased linearly. In this sense, Eq. (5) was used to calculate the endurance at cruise condition, where C_{min} represents the battery minimum capacity that can be reached in a safety margin and I_b is the battery current. The former was supposed to be 20% of the total battery capacity because lithium-based batteries can be damaged if discharged more than 80% [42]. On the other hand, I_b is a function of the motor current, avionics current, and internal resistance. Its calculation is further explained in Ref. [36], and, hence, it will not be addressed in this work. The numeric value (0.06) in Eq. (5) represents a unit conversion factor because the capacity of batteries is commonly given in milliamperes-hour, I_b in amperes, and the computed time is given in minutes. It is important to highlight that only a single battery device was considered and its number of cells was determined based on the voltage required by the motor. The range was calculated, by using the cruise speed the endurance through the assumption of a rectilinear displacement:

$$E = 0.06 \left(\frac{C_b - C_{min}}{I_b} \right) [\text{min}] \quad (5)$$

3. Results and discussion

In this section, the methodology previously explained is implemented to set the propulsion configurations for wetland monitoring at the Andean highlands. The obtained results from the UAV conceptual design, aerodynamic assessment, electric propulsion evaluation, and performance analysis are presented.

3.1 Case study

The case study was carried out for wetlands located between 3500 and 4500 masl in the Antisana volcano region from Ecuador. **Table 2** enlists some of the key operating conditions and design requirements that the aerial platform needs to fulfill in order to ensure a successful performance. Both cruise and stall speeds were set to ensure good-quality data gathering [43]. The payload mass was set not to exceed 1 kg after making a brief survey of common sensors (**Table 1**) that UAVs employ for forest monitoring [6]. These data will serve to determine the starting design point by means of the constraint analysis. It is important to mention that the maximum speed was set to be 1.25 times the cruise speed [26].

Parameter	Lower bound	Upper bound
Cruise speed [m/s]	18	22
Maximum speed [m/s]	22	26
Stall speed [m/s]	10	15
Absolute ceiling [m]	3500	4500
Aspect ratio *	4.5	5.5
Payload mass [kg]	1	1

*The aspect ratio (AR) is defined as the ratio between the wing span and its mean aerodynamic chord [33].

Table 2.
Operating conditions and design requirements.

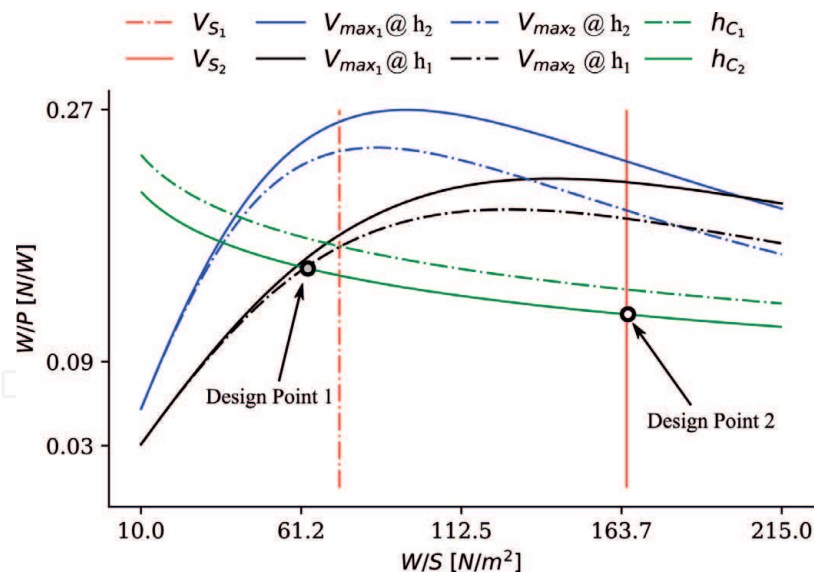


Figure 4.
 Constraint analysis to determine multiple design points.

3.2 Conceptual model

The constraint analysis illustrated in **Figure 4** shows the variation of the weight-to-power ratio (W/P) with respect to the wing loading (W/S) for various performance parameters such as the maximum speed (V_{max}), stall speed (V_s), and ceiling altitude (h_c) [26, 28]. The intersection of these curves enables to define an acceptable region of design and hence, establish a starting point for the aircraft initial sizing. It is worth to mention that for a propeller-driven aircraft, the acceptable region is located below the set of the aforesaid curves. A higher relation W/P is beneficial because this yields the smallest electric motor in terms of power required [26]; however, this is limited by the stall speed for each case. For this work, as the maximum velocity (V_{max}) function depends on the air density, a curve for each flight altitude analyzed (**Table 2**) was drawn. Thus, a total of four plots were sketched, involving two values of V_{max} at two different flight altitudes (h_c).

Two design points were defined within a permissible range of wing loading for small UAVs [27, 44] while maintaining a weight-to-power ratio as high as possible. The W/S range was established by considering the strong linkage between the structural and aerodynamic behavior of the airplane. These design points will allow to investigate the variation of wing planform area and propulsion power for different design requirements and operating conditions (**Table 2**) to contrast distinct scenarios. Note that the propulsion power computed through the constraint analysis (**Table 3**) is a preliminary estimate. A more accurate value is calculated once the geometrical parameters and the aerodynamic coefficients are defined.

Afterwards, the entire airframe (wing and fuselage) was outlined through classical methods of fixed-wing aircraft design [26]. Major geometrical parameters were obtained with respect to the preliminary weight (W_{TOP}) and wing planform area (S), previously computed in the constraint analysis. Moreover, non-dimensional parameters such as wing aspect ratio (AR) and taper ratio⁵ (λ) were initially established with regard to similar UAV architectures [12] and permissible ranges for this application [26]. The airfoil selected was the NACA 64A210 because

⁵ The taper ratio (λ) is defined as the ration between the tip chord and the root chord of a wing.

Parameter	Design point 1 case A	Design point 2 case B
Wing loading [N/m ²]	87.97	165.37
Power loading [N/W]	0.145	0.141
Reference area [m ²]	0.52	0.19
Wingspan [m]	1.60	0.99
Aspect ratio	4.96	5.22
Preliminary W_{TO} [N]	33	20
Preliminary power required [W]	224	244

Table 3.
Initial sizing parameters obtained from the constraint analysis.

it has proven to be suitable for small BWB models [45]. No twist angle was considered for this study. Main parameters from the initial sizing stage are summarized in **Table 3**.

The geometrical parameters from **Table 3** were employed to generate a three-dimensional shape of the proposed airframes as depicted in **Figure 5**. This resulted in two different models whose primary difference is the size.

3.3 Aerodynamic assessment

The aerodynamic coefficients from both design concepts were estimated using the AVL open-source software. For this aim, these coefficients were obtained regarding the variation of the attack (α), that is the angle between the freestream velocity vector and the flight path as shown in **Figure 6**.

The drag polar obtained from the aerodynamic assessment of both conceptual UAV models (**Table 3** and **Figure 5**) is depicted in **Figure 7**. In this sense, the left plot illustrates the variation of both lift (C_L) and drag (C_D) coefficients with respect to the angle of attack. It is important to highlight that the AVL software employs the Vortex Lattice Theory to predict the aerodynamic coefficients and, thus, it does not predict the stall behavior at high angles of attack. In addition, this code does not calculate the zero-lift drag coefficient, and, therefore, the total drag coefficient was estimated through semiempirical methods [40, 46].

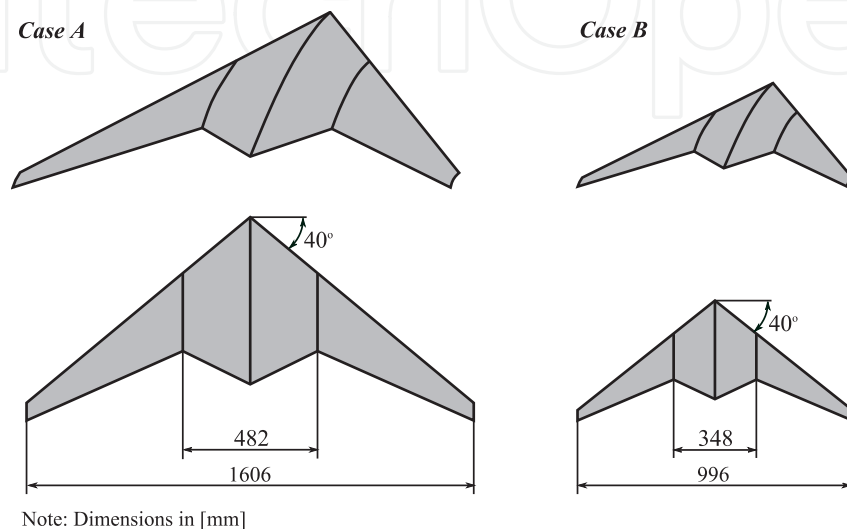


Figure 5.
Graphical representation of BWB airframe for two design cases (dimension in mm).

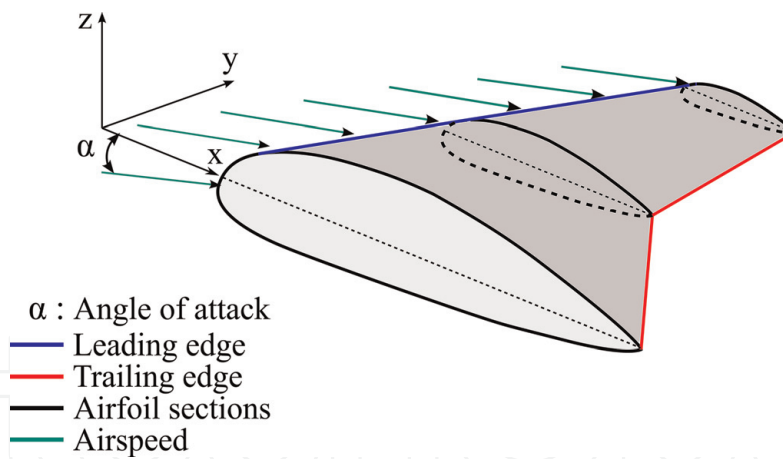


Figure 6.
 Angle of attack between the freestream and a half wing.

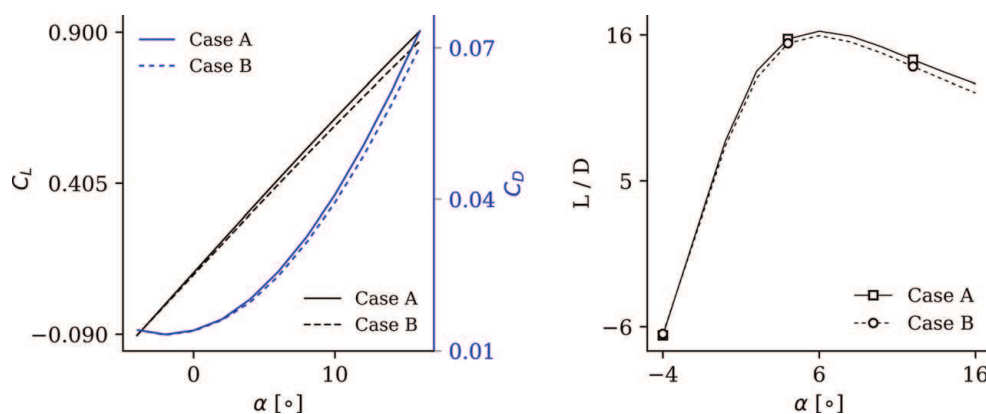


Figure 7.
 Drag polars of UAV conceptual models.

On the other hand, the right plot of **Figure 7** depicts the aerodynamic relation lift-to-drag (L/D) as a function of the angle of attack. This relation is a common way of reflecting the aerodynamic efficiency of an aircraft as a function of geometrical configuration and flight conditions. Moreover, this relation is highly important because it directly impacts on the endurance and range. The maximum L/D ratios obtained for cases A and B are 15.5 and 15.8, respectively. For this case, the minimum drag condition has been set for the cruise flight regime [35]. Finally, as seen in **Figure 7**, an L/D ratio of 8 at cruise condition is expected for both cases, which is in accordance with commercial UAV models [6].

On the other hand, the target power available, estimated by means of Eq. (3), was 302 W for both cases. This value is the same for cases A and B because their weight, aerodynamic coefficients, and operating conditions are almost equal, and hence an equivalent behavior is expected. Note that the estimated value through Eq. (3) is greater than the preliminary power required computed in the constraint analysis (**Table 3**) because during the initial sizing stage, several parameters were assumed based on historical and statistical data. Therefore, the power required calculated with Eq. (3) is more accurate because it considers the real performance and geometrical characteristics of the conceptual UAV.

3.4 Propulsion modelling

To investigate the integration of electric distributed propulsion into small UAV concepts, the available space on the trailing edge of the fuselage, as shown in

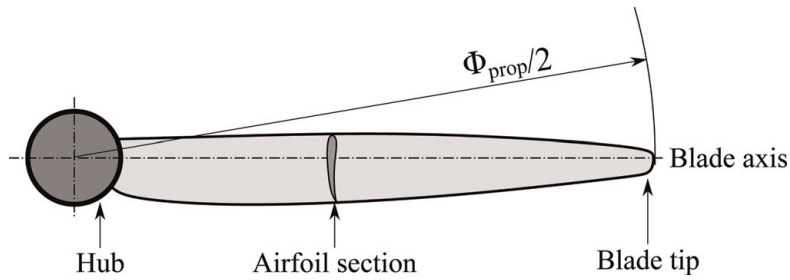


Figure 8.
Main components of propeller geometry.

Cases	N_p				
	1	2	3		
Case A	$T_{req,T} = 20.1$ [N] @ 15 [m/s]	$T_{req,i}$ [N]	20.10	10.05	6.70
		Φ_{prop} [in]	18.00	8.50	5.50
Case B	$T_{req,T} = 20.1$ [N] @ 15 [m/s]	$T_{req,i}$ [N]	20.10	10.05	6.70
		Φ_{prop} [in]	13.00	6.00	3.75

Table 4.
Thrust required for distributed propulsion.

Figures 1 and 6 has been considered. This allows estimating a suitable diameter for the propeller Φ_{prop} (**Figure 8**) and setting the quantity of motors that fits adequately the available space and generate the power needed.

The thrust that each propeller must generate, in conjunction with their diameter, is presented in **Table 4** for both cases (A and B) with three distinct configurations: single and distributed propulsion with double and triple propulsors. Note that when the propulsion system possesses more than one propulsor, the thrust required per propeller ($T_{req,i}$) is obtained by dividing the total thrust required (T_{req}) by the number of installed propellers. Besides, it is important to mention that the term T_{req} was obtained by dividing the power required for the desired value for cruise speed (15 m/s for both cases).

3.4.1 Propeller selection

Tables 5 and 6 summarize the performance characteristics of selected propellers for cases A and B, respectively. The suitable models were established regarding the freestream velocity, their diameter, and the rotational speed. Special attention was paid to guarantee that the considered propeller arrangements fit the available space and, at the same time, generate the thrust required. The cruise speed was set for minimum drag condition [35].

For each propulsion set, several parameters from propellers, such as: non-dimensional coefficients (J , C_T , and C_P), efficiency, torque, shaft power, and thrust generated were extracted from the experimental database at desired operating conditions. Notice that the power available of individual propellers ($P_{A,i}$) was obtained by multiplying the power shaft for its corresponding propeller efficiency (η_p). Likewise, the total power available (P_A) is a function of the number of propellers (N_p) implemented, and it was obtained by multiplying N_p for its corresponding individual power ($P_{A,i}$). Finally, the power that battery must supply to the propulsion system was obtained by multiplying the power shaft for the

N_p	1		2		3	
Propeller	17 × 10	18 × 10	8 × 6	8 × 10	5 × 3	5 × 5
RPM × 10 ³	5	5	13	12	27	25
J	0.44	0.42	0.36	0.4	0.26	0.3
C_T	0.069	0.061	0.1078	0.1195	0.1145	0.1213
C_P	0.0415	0.0353	0.068	0.095	0.0642	0.0851
η_P	0.73	0.72	0.57	0.5	0.47	0.42
P_{shaft} [W]	432.5	499.6	294.5	320.6	238.1	249.1
$P_{A,i}$ [W]	315.7	359.7	167.9	160.3	111.9	104.6
P_A [W]	315.7	359.7	335.8	320.6	335.7	313.8
Q [Nm]	0.831	0.954	0.216	0.257	0.083	0.095
T_i [N]	20.2	22.7	10.5	10.1	7.4	6.7
T [N]	20.2	22.7	21	20.2	22.2	20.1
P_{bat} [kW]	0.432	0.499	0.589	0.641	0.714	0.747

Table 5.
Propeller selection—case A.

N_p	1		2	
Propeller	12 × 6.5	11 × 7	6 × 4	6 × 3
RPM × 10 ³	9	10	25	23
J	0.326	0.33	0.23	0.26
C_T	0.0979	0.1036	0.0949	0.1166
C_P	0.0544	0.0657	0.0473	0.0627
η_P	0.58	0.52	0.46	0.48
P_{shaft} [W]	589.1	634.5	344.5	355.7
$P_{A,i}$ [W]	335.8	329.9	158.5	170.7
P_A [W]	335.8	329.9	316.9	341.5
Q [Nm]	0.627	0.605	0.131	0.148
T_i [N]	23.1	21.5	10.8	10.9
T [N]	23.1	21.5	21.6	21.8
P_{bat} [kW]	0.589	0.634	0.689	0.711

Table 6.
Propeller selection—case B.

number of propellers implemented. Note that the shaft power and the battery power will be the same for a single propeller configuration because only one motor is considered and the electrical efficiency losses were neglected for practical purposes.

Note that, in **Tables 5** and **6**, the propeller efficiency is dramatically affected as its diameter is reduced. As observed, the lesser the propeller's size, the higher the rotational speed is needed to generate the required thrust. For instance, smaller models (e.g., three propellers 5 × 3) must operate at a high RPM (27,000) to produce the thrust required (**Table 4**). In contrast, a single larger propeller (e.g., a propeller 17 × 10) operates at lower RPM (5000) to generate the same thrust. These

aspects also reflect the variation of propeller efficiency due to its direct linkage to the cruise speed, rotational speed (ω), and propeller diameter (ϕ_{prop}) [47, 48]. In this sense, the decrease of propeller efficiency (as its diameter is lower) is attributed to the increase of the induced velocity at the propeller tips, which in turn increments the tip losses due to drag [47].

In addition, the lower propeller efficiency, the higher power that needs to be delivered by the motor (P_{shaft}). As observed in **Tables 5** and **6**, the large drop in efficiency (around 20% for the increment of one propeller) produces an increment in total power consumed. Nonetheless, the total power available (P_A) for all the cases remains almost constant, and it agrees the target power available (302 W).

Table 6 shows similar results as **Table 5**; however, it is worth to highlight that propeller efficiencies are even lower due to the smaller propeller's diameters for this case, which results in higher values of power shaft compared to case A. Additionally, note that the three-propeller configuration for this case was not assessed due to the unsuitability of allocating more than two propellers within the airframe trailing edge.

3.4.2 Motor selection

The selection of an electric motor for each set of propellers was accomplished through a catalogue-search of different manufacturers. The key parameters for motor selection and propeller-motor matching were the revolutions per minute (RPM), power shaft, and voltage constant. The latter represents a motor constant which correlates the RPMs and the operating voltage. Finally, when the set of the propeller and electric components is found, recommended values given by manufacturers for propeller pairing were used to check if the established arrangement meets the requirements.

Tables 7 and **8** present the motor devices for the propulsion configurations of cases A and B, respectively. As observed, for the distributed propulsion systems with three propellers of case A (**Table 7**) and with two propellers of case B (**Table 8**), it was not possible to find any off-the-shelf electrical motor that fulfills the propeller requirements, and, hence, they were not used in further analysis. For all favorable cases (first and second arrangements of case A and first set of case B), adequate motor models were decided, and their operating parameters were employed to size and select a suitable battery to perform a given mission.

N_p	Propeller	Motor	RPM	Battery cells	K_V	I_{m0} [A]	U_{m0} [V]	R_m [Ohm]
1	17 × 10	A40-14L V4 14-Pole	6000	6S	355	0.85	8.4	0.050
2	8 × 6	A40-12S V4 8-Pole	12,820	3S	1350	1.94	8.4	0.018
3	5 × 3	No motor matching	–	–	–	–	–	–

Table 7.
Motor selection—case A.

N_p	Propeller	Motor	RPM	Battery cells	K_V	I_{m0} [A]	U_{m0} [V]	R_m [Ohm]
1	12 × 6.5	A30 8 XL V4	9500	3S	1100	2.8	8.4	0.015
2	6 × 3	No motor matching	–	–	–	–	–	–

Table 8.
Motor selection—case B.

3.5 Performance assessment

As mentioned, the performance of an electric aerial vehicle mainly depends on the battery capacity and the total current draw supplied to the propulsion system. For this work, a single battery device was considered for each configuration, even in the case of distributed propulsion. In this way, the battery current (I_B) was computed as a function of several motor parameters such as voltage constant (K_v), no-load current (I_{m0}), no-load voltage (U_{m0}), and motor resistance (**Tables 7 and 8**). Another parameter employed for the battery selection was its nominal voltage (U_B), which is directly linked to the number of internal cells.

For case A, when a single propeller is considered, the battery voltage is almost twice the voltage of the distributed propulsion scenario. This is because a larger propeller demands higher torque to work properly, and hence a larger motor that works with a higher voltage is employed. Nonetheless, it is also observed that the current supplied by the battery to the motors (I_B) for the distributed propulsion configuration is twice the value of the single propeller set. This is because two motors that work in a parallel are employed in the first case. Moreover, it is seen that the motor of case B-1 requires a lower voltage than the case A-1, because of the difference in size of the propellers employed (**Tables 5 and 6**). The number of cells of the battery for each configuration was set according to the manufacturer suggestion. **Table 9** compiles the results of general battery characteristics such as the number of cells and total current that battery supplies.

Regarding the takeoff gross weight estimation, it can be appreciated that the higher the nominal voltage, the higher number of cells from the battery and hence the aircraft weight increases. In this sense, two different scenarios were investigated to select a battery. The first one consisted of selecting a desired capacity from commercial datasheets, and, from this, the vehicle performance was assessed. For this approach, **Table 10** and **Figure 9** present the UAV weight estimation and its breakdown for the three configurations once the battery characteristics have been outlined. Meanwhile, **Table 11** shows the estimated range and endurance under these battery characteristics.

It is interesting to note that for case A, the takeoff gross weight (W_{TO}) of the aircraft is lower when the distributed propulsion system is implemented; however, the weight fractions of the components are altered. For instance, the propulsion

Case	N_p	Cells	U_B [V]	U_{eo} [V]	I_m [A]	I_B [A]
CA-1	1	6	22.2	19.1	31.9	28.4
CA-2	2	3	11.1	10.7	32.6	63.8
CB-1	1	3	11.1	10.8	75.4	74.2

Table 9.
 Parameter for battery selection—cases A and B.

Case	N_p	W_{motor} [kg]	$W_{propeller}$ [kg]	W_{ESC} [kg]	$W_{battery}$ [kg]	$W_{fuselage}$ [kg]	$W_{payload}$ [kg]	W_{TO} [kg]
CA-1	1	0.275	0.063	0.05	2.024	0.538	1	3.95
CA-2	2	0.190	0.014	0.05	1.055	0.538	1	3.10
CB-1	1	0.177	0.041	0.06	1.055	0.118	1	2.45

Table 10.
 Weight assessment—cases A and B.

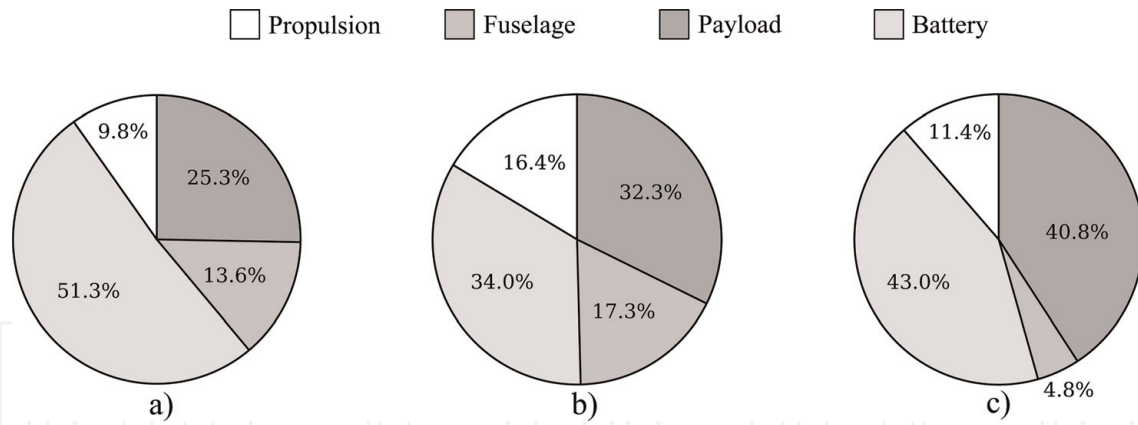


Figure 9. UAV—weight breakdown. (a) Case A-1 propeller, (b) case A-2 propeller, and (c) case B-1 propeller.

Cases	Method 1			Method 2		
	Input	Output		Input	Output	
	C_B [mAh]	E [min]	R [km]	E [min]	R [km]	C_B [mAh]
CA-1	16,000	27.1	24.39	30	27	17731
CA-2	16,000	12.0	10.8	30	27	39,892
CB-1	16,000	10.3	9.27	30	27	46,378

Table 11. Battery selection—cases A and B.

system mass fraction increments from 9.8 to 16.4%, and, in similar way, the fuselage mass fraction increases from 25.3 to 32.3%. Although the lessening of weight that resulted from the implementation of the distributed propulsion system, this is overshadowed by the lessening of the endurance and range of the aircraft because the power consumed by the motors in the distributed propulsion scenario is higher, as showed in **Table 11**.

At last, comparing the single propeller configurations (**Figure 9a** and **c**) indicates that fuselage mass fraction is decreased for case B because of its smaller geometry. Note that the battery mass fraction is lower for case B because a 3-cell battery was employed for this configuration; meanwhile, for case A, a 6-cell configuration was utilized, which results in a weight increment.

The second performance approach determined the minimum battery capacity required for a target endurance and range. **Table 11** (Method 2) shows the results for case A (one and two-propeller configuration) and case B (one-propeller configuration). As can be seen, for the same target endurance, the battery capacity for the distributed propulsion configuration is dramatically raised compared with the single propeller setting. In other words, the capacity lasts less due to the augment of current draw that the battery must provide as consequence of the loss in propeller efficiency. When comparing the one-propeller configuration of both cases (A and B), it is observable that the endurance reduces for case B because of the aerodynamic and propulsion drawbacks arising from a lesser wetted area and lower efficiency of the propeller.

The results from the second method of performance assessment showed that the required battery capacity to accomplish a specific mission increases for distributed propulsion arrangements. As observed in **Table 11**, the capacity to perform the

same mission flight is different for all three cases because of the notable increment of the current draw (**Table 9**).

4. Summary

Wetland monitoring at the Andean highlands presents imperious needs in terms of more efficient and environmentally friendly UAV designs. The challenges imposed by the hard-operating requirements make commercial electrical small UAVs not suitable for monitoring tasks. However, their lower environmental impact and low costs encourage their improvements through the implementation of different technologies. In this context, this work has assessed the performance of two different configurations using electrical distributed propulsion system. Since for this particular application the payload required is small, the search for architectures with a large number of propulsors was not suitable, and hence the maximum number of propellers that could be allocated was set to three. The results showed that the propeller's size reduction affected dramatically its performance, outweighing the benefits in weight and propulsive efficiency. The results from the performance analysis show that endurance, range, and weight decrease for distributed propulsion configurations. The reduction on total aircraft weight is beneficial; however, this was outweighed by the lower thermal performance of the propellers, which reflected on higher total power consumption for the distributed propulsion cases. It is important to highlight that distributed propulsion may be a good option when the propeller's size does not decrease so dramatically as in the configurations studied. This aspect is a key variable in order to assess a recommendable range for distributed propulsor size, where the benefits obtained from weight, reliability, control, and aerodynamic aspects are not to be affected by the thermal propulsors' performance.

Another aspect to highlight in this study is that conversely to other aviation sectors, the small UAV category allows to implement or design an important variety of electronic propulsion components, which can be easily tailored for the operating requirements. This aspect opens up the door to generate more flexible designs which incorporates forefront technology such as thrust vectoring, boundary layer ingestion (BLI), and propulsion airframe embedded (PAE) designs, among others in exchange of moderate costs. In this sense, it is important to implement a versatile and flexible optimization methodology, which enables the assessment of different geometrical configurations accounting for the aerodynamic and propulsion integration at system engineering perspective. These routines will enable to evaluate a larger range of aircraft configurations, and it will contribute to establish ideal models that fulfill the requirements from a synergetic standpoint.

Finally, since this study was implemented at conceptual level, the distortion features and momentum reduction produced by the ingestion of the boundary layer have not been considered. Nonetheless, further studies to determine the compromise between size and propeller performance incorporating BLI aspects need to be carried out.

Acknowledgements

The authors would like to thank to Corporación Ecuatoriana para el Desarrollo de la Investigación y Academia (CEDIA) for the financial support given to the present research, development, and innovation work through its CEPRA program, especially for the CEPRA XII-2018-12 fund. Furthermore, the authors gratefully

acknowledge the financial support provided by Escuela Politécnica Nacional for the development of the internal projects: PIJ 15-11 and PIS 16-20.

Abbreviations and nomenclature

ρ_{alt}	air density at desired altitude [kg/m ³]
ω	motor/propeller rotational speed [RPM]
Φ_{prop}	propeller diameter, [in]
η_e	electric set (motor, battery, ESC) efficiency
η_{prop}	propeller efficiency
BWB	blended wing body
C_D	drag coefficient
C_L	lift coefficient
C_B	battery capacity [mAh]
C_{min}	minimum battery capacity [mAh]
E	endurance [min]
I_B	total current [A]
I_m	motor current [A]
I_{m0}	nominal no-load motor current [A]
K_V	voltage constant [RPM/V]
N_p	number of propellers
RC	rate of climb [m/s]
S	planform wing area [m ²]
P_A	power available [W]
P_R	power required [W]
P_{Rp}	preliminary power required [W]
P_{shaft}	power shaft of the motor [W]
P_{bat}	power of battery [W]
Q	torque [Nm]
T	thrust [N]
UAV	unmanned aerial vehicle
U_B	nominal battery voltage [V]
U_{m0}	nominal no-load voltage of motor [V]
U_{eo}	equivalent battery voltage [V]
V_{max}	maximum flight speed [m/s]
V_c	cruise speed [m/s]
V_s	stall speed [m/s]
W/S	wing loading [N/m ²]
W/P	weight to power ratio [N/W]
$W_{battery}$	battery weight [N]
W_{ESC}	electronic speed control weight [N]
$W_{fuselage}$	fuselage weight [N]
W_{motor}	motor weight [N]
$W_{payload}$	payload weight [N]
$W_{propeller}$	propeller weight [N]
W_{TO}	takeoff gross weight [N]
W_{TOp}	preliminary takeoff gross weight [N]

IntechOpen

IntechOpen

Author details

Esteban Valencia*, Víctor Alulema and Darío Rodríguez
Department of Mechanical Engineering, National Polytechnic School, Quito,
Ecuador

*Address all correspondence to: esteban.valencia@epn.edu.ec

IntechOpen

© 2019 The Author(s). Licensee IntechOpen. This chapter is distributed under the terms of the Creative Commons Attribution License (<http://creativecommons.org/licenses/by/3.0>), which permits unrestricted use, distribution, and reproduction in any medium, provided the original work is properly cited. 

References

- [1] Baruch Z. Ordination and classification of vegetation along an altitudinal gradient in the Venezuelan páramos. *Vegetatio*. 1984;55(2):115-126
- [2] Schoolmeester T et al. Outlook on climate change adaptation in the Tropical Andes mountains. 2016
- [3] da GABF, Norman Myers JK, Mittermeier RA, Mittermeier CG. Biodiversity Hotspots for conservation priorities. *Nature*. 2000;403
- [4] Josse CE, Cuesta F, Navarro G, Barrena V, Chacón-Moreno ESJ, Ferreira W, et al. Ecosistemas de los Andes del Norte Centro. Bolivia, Colombia, Ecuador, Perú y Venezuela. Lima: Secretaría General de la Comunidad Andina, Programa Regional ECOBONA-Intercooperation, CONDESAN-Proyecto Páramo Andino, Programa BioAndes, EcoCiencia, NatureServe, IAvH, LTA-UNALM, ICAE-ULA, CDC-UNALM, RUMBOL SRL; 2009
- [5] Buytaert W et al. Human impact on the hydrology of the Andean páramos. *Earth-Science Reviews*. 2006;79(1-2):53-72
- [6] Gundlach J. Civil and Commercial Unmanned Aircraft Systems. Washington, DC: American Institute of Aeronautics and Astronautics, Inc; 2016
- [7] Marcaccio JV, Markle CE, Chow-Fraser P. Unmanned aerial vehicles produce high-resolution, seasonally-relevant imagery for classifying wetland vegetation. *International Archives of the Photogrammetry, Remote Sensing and Spatial Information Sciences*. 2015;40(1W4):249-256
- [8] Shahbazi M, Théau J, Ménard P. Recent applications of unmanned aerial imagery in natural resource management. *GIScience Remote Sensing*. 2014;51(4):339-365
- [9] E. 38 Unmanned Systems. The E384 Mapping Drone – Event 38 Unmanned Systems. 2018. [Online]. Available from: <https://event38.com/fixed-wing/e384-mapping-drone/> [Accessed: 18-June-2018]
- [10] Parrot. Parrot DISCO FPV | Official Parrot® Site. [Online]. Available: <https://www.parrot.com/us/drones/parrot-disco-fpv#-parrot-disco-fpv> [Accessed: 12-Sep-2018]
- [11] Valencia E, Saá JM, Alulema V, Hidalgo V. Parametric study of aerodynamic integration issues in highly coupled Blended Wing Body configurations implemented in UAVs. 2018. pp. 1-15
- [12] Panagiotou P, Fotiadis-Karras S, Yakinthos K. Conceptual design of a blended wing body MALE UAV. *Aerospace Science and Technology*. 2018;73:32-47
- [13] Lehmkuehler K, Wong KC, Verstraete D. Design and test of a UAV blended wing body configuration. 28th Congr Int. Counc. Aeronaut. Sci. 2012, ICAS 2012, vol. 1. April. 2012. pp. 432-442
- [14] Panagiotou P, Yakinthos K. Parametric aerodynamic study of Blended-Wing-Body platforms at low subsonic speeds for UAV applications. In: 35th AIAA Appl. Aerodyn. Conf., no. June. 2017. pp. 1-19
- [15] Dehpanah P, Nejat A. The aerodynamic design evaluation of a blended-wing-body configuration. *Aerospace Science and Technology*. 2015;43:96-110
- [16] Leifsson L, Ko A, Mason WH, Schetz JA, Grossman B, Haftka RT. Multidisciplinary design optimization of blended-wing-body transport aircraft

with distributed propulsion. *Aerospace Science and Technology*. 2013;25(1): 16-28

[17] Hepperle M. Electric Flight– Potential and Limitations. 2012. pp. 1-30

[18] Gundlach J. *Designing Unmanned Aircraft Systems: A Comprehensive Approach*. Manassas, Virginia: American Institute of Aeronautics and Astronautics, Inc; 2011

[19] Gohardani AS. A synergistic glance at the prospects of distributed propulsion technology and the electric aircraft concept for future unmanned air vehicles and commercial/military aviation. *Progress in Aerospace Science*. 2013;57:25-70

[20] Kim HD, Perry AT, Ansell PJ. A review of distributed electric propulsion concepts for air vehicle technology. In: 2018 AIAA/IEEE Electr. Aircr. Technol. Symp. 2018

[21] Herwitz SR, Johnson LF, Dunagan SE, Higgins RG, Sullivan DV, Zheng J. Imaging from an unmanned aerial vehicle: Agricultural surveillance and decision support. *Revista de Derecho Comunitario Europeo*. 2011;39(15): 523-540

[22] Grenzdörffer G et al. The photogrammetric potential of low-cost UAVs in forestry and agriculture. *International Archives of the Photogrammetry, Remote Sensing and Spatial Information Sciences*. 2008;1: 1207-1213

[23] Al-Hajjaji K, Ezzin M, Khamdan H. *Design, Development and Evaluation of a UAV to Study Air Quality in Qatar*. Qatar; 2017

[24] Johnson LF, Herwitz S, Dunagan S, Lobitz B, Sullivan D, Slye R. Collection of ultra high spatial and spectral resolution image data over California

vineyards with a small UAV. *Biosystems Engineering*. 2013;108(4):49-61

[25] Macjke DC Jr. Systems and image database resources for UAV search and rescue applications [masters theses]. 2013. p. 115

[26] Sadraey M. *Aircraft Design: A Systems Engineering Approach*. Vol. 27 (1). New Hampshire, USA: Wiley; 2013

[27] Keane AJ, Sóbester A, Scanlan JP. *Small Unmanned Fixed-Wing Aircraft Design: A Practical Approach*. John Wiley & Sons; 2017

[28] Glizde N. Wing and engine sizing by using the matching plot technique. *Transport and Aerospace Engineering*. 2017;5(1):48-59

[29] Sóbester A, Forrester AIJ. *Aircraft Aerodynamic Design: Geometry and Optimization*. 2014

[30] Bertin JJ, Rusell C. *Aerodynamics for Engineers*, 6th ed. Harlow Essex England: Pearson, 2014

[31] Ol M, Zeune C, Logan M. Analytical/experimental comparison for small electric unmanned air vehicle propellers. In: 26th AIAA Appl. Aerodyn. Conf., no. August. 2008

[32] Brandt J, Selig M. Propeller performance data at low Reynolds numbers. In: AIAA. 2011

[33] Sadraey MH. *Aircraft Performance: An Engineering Approach*. Boca Raton: CRC Press; 2017

[34] Anderson JD. *Aircraft Performance and Design*. 2003

[35] Ruijgrok GJJ. *Elements of Airplane Performance*. 2nd ed. Leeghwaterstraat: Delft University Press; 2009

[36] Quan Q. *Introduction to Multicopter Design and Control*. 2017

[37] Drela M. DC Motor/Propeller Matching - Lab 5 Lecture Notes. 2005;6:6

[38] Avanzini G, De Angelis EL, Giulietti F. Optimal performance and sizing of a battery-powered aircraft. *Aerospace Science and Technology*. 2016;59:132-144

[39] Elekes G. A geometric inequality and the complexity of computing volume. *Discrete & Computational Geometry*. Dec. 1986;1(4):289-292

[40] Valencia EA, Hidalgo V, Rodriguez D. Parametric modelling for aerodynamic assessment of a fixed wing UAV implemented for Site Specific Management. In: 2018 AIAA Inf. Syst. Infotech @ Aerosp., no. January. 2018. pp. 1-17

[41] Traub LW. Range and endurance estimates for battery-powered aircraft. *Journal of Aircraft*. 2011;48(2):703-707

[42] Scarpino M. *Motors for Makers A Guide to Steppers, Servos, and Other Electrical Machines*; 2016

[43] Kontogiannis S, Ekaterianaris J. Design, performance evaluation and optimization of a UAV. *Aerospace Science and Technology*. 2013;January: 339-350

[44] Sóbester A, Forrester AIJ. *Aircraft Aerodynamic Design: Geometry and Optimization*. 2014

[45] Shim HJ, Park SO. Low-speed wind-tunnel test results of a BWB-UCAV model. *Procedia Engineering*. 2013;67: 50-58

[46] Gur O, Mason WH, Schetz JA. Full-configuration drag estimation. *Journal of Aircraft*. 2010;47(4):1356-1367

[47] Filippone A. *Advanced Aircraft Flight Performance*. 2010

[48] Torenbeek E. *Synthesis of Subsonic Airplane Design*. Dordrecht: Springer Netherlands, 1982